

Plasmons in a Planar Graphene Superlattice

P. V. Ratnikov^a and A. P. Silin^{a,b}

^a*Lebedev Physical Institute, Russian Academy of Sciences, Leninskii pr. 53, Moscow, 119991 Russia*

^b*Moscow Institute of Physics and Technology (State University),*

Institutskii per. 9, Dolgoprudnyi, Moscow region, 141700 Russia

e-mail: ratnikov@lpi.ru

Received July 3, 2015; in final form, September 16, 2015

Plasmon collective excitations are studied in a planar graphene superlattice formed by periodically alternating regions of gapless graphene and of its gapped modification. The plasmon dispersion law is determined both for the quasi-one-dimensional case (the Fermi level is located within the minigap) and for the quasi-two-dimensional case (the Fermi level is located within the miniband). The problem concerning the absorption of modulated electromagnetic radiation at the excitation of plasmons is also considered.

DOI: 10.1134/S0021364015230137

1. INTRODUCTION

Graphene (a two-dimensional carbon material) has been actively studied both theoretically and experimentally for more than ten years. In recent years, graphene nanostructures have become a forefront issue. The usage of collective excitations (plasmons) in these systems promises new advantages for the tunable absorption of electromagnetic radiation. The plasmon-induced enhancement of light absorption within the middle infrared range was observed for the heterostructure formed by graphene strips [1].

The plasmon-type oscillations in spatially uniform systems with different dimensionalities having charge carriers with a linear dispersion law were studied in [2], where the tunneling of charge carriers was neglected. Such approximation is similar to the tight-binding approximation in the band structure theory for crystals.

In [3], the plasma oscillations of massless Dirac electrons in a planar superlattice were studied. The Dirac plasma was assumed to be weakly modulated. This picture is similar to the weak-binding approximation. The spectrum of plasma oscillations and the related absorption intensity for electromagnetic waves were determined by the methods of electrodynamics of continuous media.

In this paper, we present the calculations of the plasmon dispersion law in planar graphene superlattices. The superlattices under study are formed by alternating strips of gapless graphene and of its gapped modifications. The latter can be produced using the main property of graphene, namely, its two-dimensionality. For this, there exist two possible ways: (i) choos-

ing the material of the substrate on which graphene is deposited and (ii) depositing atoms or molecules, e.g., hydrogen atoms [4] or CrO₃ molecules [5] on the surface of a graphene sheet. Several gapped modifications of graphene with the band gap ranging from about 10 meV to 1 eV have been already obtained.

In the superlattice under study, the charge carriers effectively acquire a nonzero mass. Their dispersion law becomes nonlinear. The system is similar to a relativistic plasma in a low-dimensional space.

Plasma waves in the graphene superlattice in the presence of a high dc electric field were recently studied in [6] in the random phase approximation. The same authors [7] studied numerically the plasmon dispersion law in the planar graphene superlattice. In our work, we obtain explicit analytical results for the plasmon dispersion law in the planar graphene superlattice.

2. EFFECTIVE MODEL DESCRIPTION OF THE SUPERLATTICE

2.1. Fundamentals of the Model Description of the Superlattice

The main concepts concerning the planar superlattices based on gapless graphene and on its gapped modifications were reported in [8].

Let x and y axes be normal and parallel to the interfaces, respectively (Fig. 1). The charge carriers in a superlattice are described by the Dirac equation

$$(\mathbf{v}_F \boldsymbol{\sigma} \hat{\mathbf{p}} + \sigma_z \Delta + V) \Psi(x, y) = E \Psi(x, y), \quad (1)$$

where $\mathbf{v}_F \approx 10^8$ cm/s is the Fermi velocity; $\boldsymbol{\sigma} = (\sigma_x, \sigma_y)$ and σ_z are the Pauli matrices; and $\hat{\mathbf{p}} = -i\nabla$ is the mo-

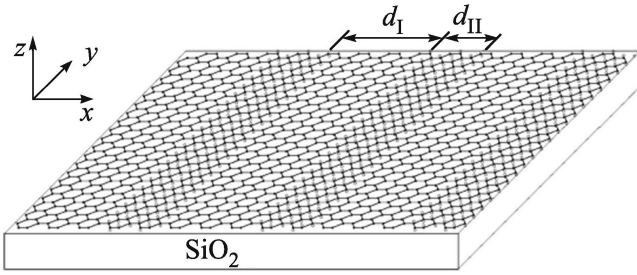


Fig. 1. Example of an array under study: graphene sheet on SiO₂ substrate with hydrogen atoms periodically deposited on graphene strips (graphene-graphane superlattice).

momentum operator (we use units with $\hbar = 1$). The half-width Δ of the band gap and the work function V are periodically modulated along the x axis

$$\Delta = \begin{cases} 0, & d(n-1) < x < -d_{\text{II}} + dn, \\ \Delta_0, & -d_{\text{II}} + dn < x < dn, \end{cases} \quad (2)$$

$$V = \begin{cases} 0, & d(n-1) < x < -d_{\text{II}} + dn, \\ V_0, & -d_{\text{II}} + dn < x < dn. \end{cases}$$

where n is an integer enumerating the superlattice supercells; d_I and d_{II} are the widths of strips of gapless and gapped graphene, respectively; and $d = d_I + d_{\text{II}}$ is the period of the superlattice (see Fig. 1). The profile of the potential is depicted in Fig. 2.

In this work, we assume that v_F has the same value over the whole superlattice. In [9], we considered a new type of superlattice with alternating Fermi velocity.

The motion of charge carriers along the y axis is free and the wavefunction has the form $\Psi(x, y) = \psi(x)e^{ik_y y}$.

The dispersion relation for decaying solution (1) within the potential barriers has the form [8]

$$\frac{v_F^2 k_2^2 - v_F^2 k_1^2 + V_0^2 - \Delta_0^2}{2v_F^2 k_1 k_2} \sinh(k_2 d_{\text{II}}) \sin(k_1 d_I) + \cosh(k_2 d_{\text{II}}) \cos(k_1 d_I) = \cos(k_x d), \quad (3)$$

where k_1 and k_2 are related to the energy E by the formulas

$$E = \pm v_F \sqrt{k_y^2 + k_1^2}, \quad (4)$$

$$E = V_0 \pm \sqrt{\Delta_0^2 + v_F^2 k_y^2 - v_F^2 k_2^2}.$$

For the further analysis, it is difficult to use the exact spectrum of charge carriers determined by finding the numerical solution of Eq. (3). We suggest using the effective spectrum (the spectrum of a model narrow-gap semiconductor).

2.2. Effective Theory

We should distinguish two cases: (i) the Fermi level falls within one of the minigaps and (ii) the Fermi level is located within one of the minibands.

In the former case, all minibands lying below the Fermi level are completely occupied and the oscillations

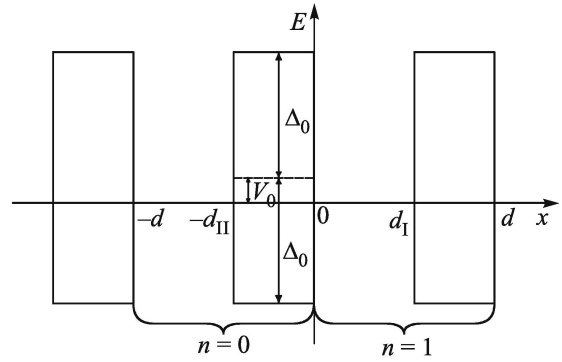


Fig. 2. Model periodic one-dimensional Kronig-Penney potential for the superlattice under study.

of the electron (hole) density occur only in the direction of the free motion of charge carriers (along the normal to the direction of the voltage applied across the superlattice). This is a quasi-one-dimensional motion.

In the latter case, the miniband containing the Fermi level is occupied only partially, whereas all lower bands (if such bands exist) are completely occupied. In the partially occupied miniband, the oscillations of electron (hole) density can also occur along the direction of the voltage applied across the superlattice. This is a quasi-two-dimensional motion.

Then, for simplicity, we consider the situation with the filling (complete or partial) of only one lowest electron miniband or the highest hole miniband.

2.2.1. Quasi-one-dimensional case (completely occupied miniband). At sufficiently large values of Δ_0 and d_{II} , the minibands are rather narrow (we shall specify this condition below). In this case, the energy spectrum of charge carriers is similar to that characteristic of a quasi-one-dimensional narrow-gap semiconductor

$$E \approx V_{\text{eff}} \pm \sqrt{\Delta_{\text{eff}}^2 + v_F^2 k_y^2}. \quad (5)$$

The parameters Δ_{eff} and V_{eff} play the role of the effective band gap and the effective work function, respectively. The charge carriers have the effective mass

$$m^* = \frac{\Delta_{\text{eff}}}{v_F^2}. \quad (6)$$

Using dispersion relation (3) and assuming that $|V_{\text{eff}}| < \Delta_{\text{eff}} \ll \Delta_0$, we can easily deduce the following estimates for Δ_{eff} and V_{eff} :

$$\Delta_{\text{eff}} = \frac{\pi v_F}{2d_I} \left[1 - \frac{v_F}{d_I \Delta_0} \right], \quad (7)$$

$$V_{\text{eff}} = \frac{v_F}{d_I \Delta_0} V_0.$$

In the case under study, the minibands have an exponentially small width owing to an exponentially small probability for charge carriers to tunnel through the barriers. In this limit, we obtain the following estimate for the miniband width:

$$\delta E = \frac{4v_F}{d_I} \exp\left(-\frac{d_{\text{II}}}{v_F} \Delta_0\right). \quad (8)$$

The condition defining the narrow minibands is $\delta E \ll \Delta_{\text{eff}}$. Comparing the expression for Δ_{eff} in Eqs. (7) with Eq. (8), we find the condition $\Delta_0 \gtrsim 2v_F/d_{\text{II}}$.

Let us write the effective Hamiltonian corresponding to the approximate dispersion law given by Eq. (5) as the Dirac Hamiltonian in terms of 2×2 matrices

$$\hat{H}_{\text{eff}}^{(1D)} = v_F \sigma_y \hat{p}_y - \sigma_z \Delta_{\text{eff}} + V_{\text{eff}}. \quad (9)$$

Here, the minus sign in front of the second term is placed for convenience of further calculations. This does not affect the final results since there Δ_{eff} is squared.

In the zeroth order approximation, the Green's function describing the free propagation of charge carriers along the gapless graphene strips has the form of the inverse operator [10]

$$\hat{G}_0^{(1D)}(k_y, \omega) = \left[\omega + \mu - \hat{H}_{\text{eff}}^{(1D)} \right]^{-1}, \quad (10)$$

where μ is the chemical potential (coincides with the Fermi energy).

Substituting Eq. (9) into operator (10), we can explicitly write the Green's function taking into account the rules of path tracing around the poles

$$\begin{aligned} \hat{G}_0^{(1D)}(k_y, \omega) &= \frac{1}{2\varepsilon_{k_y}} \\ &\times \sum_{s=\pm 1} s \frac{\omega + \tilde{\mu} - \sigma_z \Delta_{\text{eff}} + v_F \sigma_y k_y}{\omega + \tilde{\mu} - s\varepsilon_{k_y} - i\delta \text{sgn}(\tilde{\mu} - s\varepsilon_{k_y})}, \end{aligned} \quad (11)$$

where $\tilde{\mu} = \mu - V_{\text{eff}}$ and $\varepsilon_{k_y} = \sqrt{\Delta_{\text{eff}}^2 + v_F^2 k_y^2}$, $\delta \rightarrow +0$.

The value of $\tilde{\mu}$ is related to the Fermi momentum p_F as follows:

$$|\tilde{\mu}| = \sqrt{\Delta_{\text{eff}}^2 + v_F^2 p_F^2}. \quad (12)$$

The one-dimensional Fermi momentum is expressed in terms of the charge carrier density

$$p_F = \frac{\pi}{g} n_2 D d, \quad (13)$$

where $g = g_s g_v$ is the degeneracy order ($g_s = 2$ is the spin degeneracy order and $g_v = 2$ is the valley degeneracy order).

2.2.1. Quasi-two-dimensional case (partially occupied miniband). In the quasi-two-dimensional case, in addition to the free motion along the gapless graphene strips, charge carriers move across the potential barriers. These types of motion occur at different velocities: at v_{\parallel} for the free motion and at a much lower velocity $v_{\perp} \ll v_{\parallel}$ (since the probability of tunneling through the potential barrier is small). This means the quasi-two-dimensional anisotropic motion of charge carriers. The corresponding values of v_{\perp} and v_{\parallel} are selected by fitting the approximate dispersion law

$$E \approx V_{eff} \pm \sqrt{\Delta_{eff}^2 + v_{\perp}^2 k_x^2 + v_{\parallel}^2 k_y^2}. \quad (14)$$

The energy spectrum is similar to that of an anisotropic narrow-band semiconductor with the effective masses $m_{\perp}^* = \Delta_{\text{eff}}/v_{\perp}^2 \neq m_{\parallel}^* = \Delta_{\text{eff}}/v_{\parallel}^2$. The temperature should be sufficiently low, $T \ll \delta E$.

The effective Hamiltonian with eigenvalues (14) has the form

$$\hat{H}_{\text{eff}}^{(2D)} = v_{\perp} \sigma_x \hat{p}_x + v_{\parallel} \sigma_y \hat{p}_y - \sigma_z \Delta_{\text{eff}} + V_{\text{eff}}. \quad (15)$$

The Green's function is determined as inverse operator (10) with the Hamiltonian

$$\begin{aligned} \hat{G}_0^{(2D)}(\mathbf{k}, \omega) &= \frac{1}{2\varepsilon_{\mathbf{k}}} \\ &\times \sum_{s=\pm 1} s \frac{\omega + \tilde{\mu} - \sigma_z \Delta_{\text{eff}} + v_{\perp} \sigma_x k_x + v_{\parallel} \sigma_y k_y}{\omega + \tilde{\mu} - s\varepsilon_{\mathbf{k}} - i\delta \text{sgn}(\tilde{\mu} - s\varepsilon_{\mathbf{k}})}, \end{aligned} \quad (16)$$

where $\varepsilon_{\mathbf{k}} = \sqrt{\Delta_{\text{eff}}^2 + v_{\perp}^2 k_x^2 + v_{\parallel}^2 k_y^2}$.

3. PLASMONS

3.1. Coulomb Interaction

In the quasi-one-dimensional case, the charge carriers do not move between the gapless graphene strips. The Coulomb interaction is similar to that for charge carriers in a periodic planar array formed by parallel filaments. In such array, the Coulomb interaction of charges located at two filaments separated by the distance nd reads [11]

$$V(k_y, n) = 2\tilde{e}^2 K_0(d|nk_y|), \quad (17)$$

where d is the distance between the gapless graphene strips (it coincides with the period of the superlattice); n is the number of a strip (it can be considered as that coinciding with the number of a supercell in the superlattice shown in Fig. 2); $\tilde{e}^2 = e^2/\varepsilon_{\text{eff}}$, where $\varepsilon_{\text{eff}} = (\varepsilon_1 + \varepsilon_2)/2$ is the effective static dielectric constant determined by the static dielectric constants ε_1 and ε_2 of the media surrounding the graphene (e.g., vacuum and the substrate material); and $K_0(x)$ is the modified Bessel function of the second kind.

Now, we can make the transformation from the discrete variable n denoting the strip number to the dimensionless transverse momentum $\theta = k_x d$ ($-\pi \leq \theta \leq \pi$), as was done in [11]

$$\begin{aligned} V(k_y, \theta) &= \sum_{n=-\infty}^{\infty} V(k_y, n) e^{in\theta} \\ &= 2\tilde{e}^2 K_0\left(\frac{d_I}{2}|k_y|\right) + 4\tilde{e}^2 \sum_{n=1}^{\infty} \cos(n\theta) K_0(nd|k_y|). \end{aligned} \quad (18)$$

In the case of the narrow barrier, which is of main interest to us, expression (18) becomes simpler ($d_{\text{II}} \ll d_I$) [11]

$$\begin{aligned} V(k_y, \theta) &= 2\tilde{e}^2 \ln \frac{d}{\pi d_I} \\ &+ \left[-2C - 2\psi\left(\frac{\theta}{2\pi} + \frac{1}{2}\right) + \pi \tan \frac{\theta}{2} \right] \tilde{e}^2 + o(k_y d), \end{aligned} \quad (19)$$

where $C = 0.577\dots$ is the Euler constant and $\psi(x)$ is the Euler ψ function. At the miniband boundaries, we have

$$V(k_y, \pm\pi) = 2\tilde{e}^2 \ln \frac{d}{\pi d_I} + \frac{2\pi\tilde{e}^2}{|k_y|d} + o(k_y d). \quad (20)$$

3.2. Polarization Operator

In the calculations of the plasmon frequencies using the diagram technique, we should distinguish two specific cases: (i) the quasi-one-dimensional isotropic case (the corresponding Green's function is determined in Subsection 2.2.1) and (ii) the quasi-two-dimensional anisotropic case (the corresponding Green's function is determined in Subsection 2.2.2). Hence, we have two expressions for the polarization operator needed for finding the plasmon dispersion law.

3.2.1. Quasi-one-dimensional polarization operator. The polarization operator is represented by the loop diagram (Fig. 3) and is given by the expression

$$\begin{aligned} \Pi^{(1D)}(k_y, \omega) = & -ig \int \frac{dp_y}{2\pi} \\ & \times \int \frac{d\varepsilon}{2\pi} \text{Tr} \left\{ \widehat{G}_0^{(1D)}(p_y, \varepsilon) \widehat{G}_0^{(1D)}(p_y + k_y, \varepsilon + \omega) \right\}. \end{aligned} \quad (21)$$

Similar to the situation in quantum electrodynamics (QED), expression (21) should be renormalized. However, the many-body problem in solids has its specific features. Although the bare electron and hole spectra are identical to those of electrons and positrons in QED, the set of parameters and the laws involved in these renormalizations are different [12, 13].

The renormalization of the polarization operator is reduced to the condition [14]

$$\Pi_{\text{Ren}}^{(1D)}(k_y, \omega) = \Pi^{(1D)}(k_y, \omega) - \Pi^{(1D)}(k_y, \omega) \Big|_{n_{2D} \rightarrow 0}. \quad (22)$$

We are interested in plasmons (the long-wavelength collective excitations); therefore, it is sufficient to determine the polarization operator at low k_y and ω values:

$$|k_y| \ll \frac{\Delta_{\text{eff}}}{v_F}, \quad |\omega| \ll \Delta_{\text{eff}}. \quad (23)$$

As we can see below, the plasmon frequencies are low because of low k_y values (the plasmon dispersion law for low-dimensional systems).

In the quasi-one-dimensional case, the real part of the renormalized polarization operator at low crystal momenta (the expansion is performed up to terms of the order of k_y^2) and frequencies specified by Eqs. (23) is given by the expression

$$\begin{aligned} \text{Re} \Pi_{\text{Ren}}^{(1D)}(k_y, \omega) = & \frac{g}{2\pi} \\ & \times \left\{ -\Lambda_1 + \frac{|k_y|}{|\widetilde{\mu}|} + \frac{2v_F^2 p_F k_y^2}{|\widetilde{\mu}| \omega^2} + \frac{v_F^4 p_F^3 k_y^2}{3|\widetilde{\mu}|^3 \Delta_{\text{eff}}^2} \right\}, \end{aligned} \quad (24)$$

where

$$\Lambda_1 = \frac{1}{v_F} \ln \frac{|\widetilde{\mu}| + v_F p_F}{|\widetilde{\mu}| - v_F p_F}. \quad (25)$$

Note that Λ_1 is positive, is independent of both k_y and ω , and appears in Eq. (24) with the negative sign. It is easy to see that this term in Eq. (24) results in a pronounced (background) screening. Hence, Λ_1 should

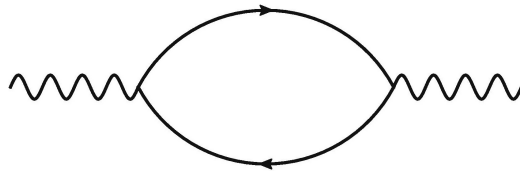


Fig. 3. Loop diagram.

be omitted. In addition, in the limit $\Delta_{\text{eff}} \rightarrow 0$, it leads to a logarithmic divergence.

The term linear in $|k_y|$ actually turns out to be small in comparison to the third term, which is formally of the order of k_y^2 . In the denominator of the third term, we have ω^2 , and $\omega \gtrsim v_F |k_y|$, but it is still of the same order as $v_F |k_y|$. Therefore, in spite of the formally higher order of the third term, it turns out to be larger than the second one.

Expression (24) is derived under the assumption that $v_F |k_y| \lesssim |\omega| \ll \Delta_{\text{eff}}$. At the same time, we assume that $v_F p_F \ll \Delta_{\text{eff}}$ (the case of a low charge carrier density) or, at least, $v_F p_F \lesssim \Delta_{\text{eff}}$ (the case of a moderate charge carrier density). Therefore, in contrast to the third term, the last term in Eq. (24) is smaller than or of the order of $\omega^2 / \Delta_{\text{eff}}^2$ in the case of a moderate charge carrier density and of a higher order in the case of a low charge carrier density. Therefore, we can neglect the last term in Eq. (24).

Finally, we find

$$\text{Re} \Pi_{\text{Ren}}^{(1D)}(k_y, \omega) = \frac{g v_F^2 p_F k_y^2}{\pi |\widetilde{\mu}| \omega^2}. \quad (26)$$

The imaginary part of $\Pi_{\text{Ren}}^{(1D)}(k_y, \omega)$ vanishes within the range

$$v_F |k_y| < |\omega| < \sqrt{4\Delta_{\text{eff}}^2 + v_F^2 k_y^2}, \quad (27)$$

which is in agreement with the well-known result for relativistic plasma [15].

3.2.2. Quasi-two-dimensional polarization operator. In the quasi-two-dimensional anisotropic case, the polarization operator is represented similarly to Eq. (21) as

$$\begin{aligned} \Pi^{(2D)}(\mathbf{k}, \omega) = & -igd \int \frac{d^2 p}{(2\pi)^2} \\ & \times \int \frac{d\varepsilon}{2\pi} \text{Tr} \left\{ \widehat{G}_0^{(2D)}(\mathbf{p}, \varepsilon) \widehat{G}_0^{(2D)}(\mathbf{p} + \mathbf{k}, \varepsilon + \omega) \right\}. \end{aligned} \quad (28)$$

The renormalization condition in the form of Eq. (22) should also be imposed on polarization operator (28). At low crystal momenta (we retain the terms of the order of k_x^2 and k_y^2) and low frequencies specified by Eqs. (23), the real part of the renormalized polarization operator has the form

$$\begin{aligned} \text{Re} \Pi_{\text{Ren}}^{(2D)}(\mathbf{k}, \omega) = & \frac{gd}{2\pi} \left\{ -\Lambda_2 + \frac{v_{\perp}^2 k_x^2 + v_{\parallel}^2 k_y^2}{v_{\perp} v_{\parallel}} \right. \\ & \times \left. \left[\frac{\widetilde{\mu}^2 - \Delta_{\text{eff}}^2}{2|\widetilde{\mu}| \omega^2} + \frac{1}{6\Delta_{\text{eff}}} \left(1 - \frac{3\Delta_{\text{eff}}}{2|\widetilde{\mu}|} + \frac{\Delta_{\text{eff}}^3}{2|\widetilde{\mu}|^3} \right) \right] \right\}, \end{aligned} \quad (29)$$

which includes the positive parameter

$$\Lambda_2 = \frac{|\tilde{\mu}| - \Delta_{\text{eff}}}{\mathbf{v}_\perp \mathbf{v}_\parallel}. \quad (30)$$

This parameter should also be omitted for the same reasons as in the case of Λ_1 in Eq. (24). The second term in the square brackets is smaller than the first one by a factor of $\omega^2/(\tilde{\mu}^2 - \Delta_{\text{eff}}^2)$ and, therefore, can also be omitted. Thus, we obtain

$$\text{Re } \Pi_{\text{Ren}}^{(2D)}(\mathbf{k}, \omega) = \frac{gd}{4\pi} \frac{\mathbf{v}_\perp^2 k_x^2 + \mathbf{v}_\parallel^2 k_y^2}{\mathbf{v}_\perp \mathbf{v}_\parallel} \frac{\tilde{\mu}^2 - \Delta_{\text{eff}}^2}{|\tilde{\mu}| \omega^2}. \quad (31)$$

The imaginary part of $\Pi_{\text{Ren}}^{(2D)}(\mathbf{k}, \omega)$ vanishes within the range

$$\sqrt{\mathbf{v}_\perp^2 k_x^2 + \mathbf{v}_\parallel^2 k_y^2} < |\omega| < \sqrt{4\Delta_{\text{eff}}^2 + \mathbf{v}_\perp^2 k_x^2 + \mathbf{v}_\parallel^2 k_y^2}. \quad (32)$$

3.3. Dispersion Law for Plasmons

In the random phase approximation, the dispersion law for plasmons is determined by the equation

$$1 - V(\mathbf{k})\Pi(\mathbf{k}, \omega) = 0. \quad (33)$$

When the Fermi level falls within the minigap, Eq. (26) for the polarization operator $\Pi(\mathbf{k}, \omega)$ and Eq. (18) for the Coulomb interaction should be substituted into Eq. (33). When the Fermi level falls within the miniband, Eq. (31) for the polarization operator $\Pi(\mathbf{k}, \omega)$ and Eq. (18) with $\theta = k_x d$ for the Coulomb interaction should be substituted into Eq. (33). In the former case, we obtain

$$\omega_{pl}^{(1D)}(k_y, \theta) = \mathbf{v}_F |k_y| \sqrt{\frac{g p_F}{\pi |\tilde{\mu}|}} V(k_y, \theta). \quad (34)$$

In the latter case, we have

$$\omega_{pl}^{(2D)}(\mathbf{k}) = \sqrt{\mathbf{v}_\perp^2 k_x^2 + \mathbf{v}_\parallel^2 k_y^2} \sqrt{\frac{gd}{4\pi} \frac{\tilde{\mu}^2 - \Delta_{\text{eff}}^2}{\mathbf{v}_\perp \mathbf{v}_\parallel |\tilde{\mu}|}} V(\mathbf{k}). \quad (35)$$

In the case of closely spaced strips of gapless graphene, expression (34) at the boundary of the plasmon band gives the square-root plasmon dispersion law characteristic of two-dimensional systems:

$$\omega_{pl}^{(1D)}(k_y) = \mathbf{v}_F \sqrt{\frac{2\pi n_{2D} \tilde{e}^2}{|\tilde{\mu}|}} |k_y|. \quad (36)$$

At low k_y values, we retain only the second term in Eq. (20) for the Coulomb interaction.

However, it follows from Eq. (34) in this case that the plasmon dispersion law remains acoustic for nearly the whole plasmon band (almost for all θ values),

$$\omega_{pl}^{(1D)}(k_y, \theta) = \mathbf{v}_F |k_y| \sqrt{\frac{2g\tilde{e}^2 p_F}{\pi |\tilde{\mu}|}} f(\theta), \quad (37)$$

where

$$f(\theta) = \ln \frac{d}{\pi d_I} - C - \psi \left(\frac{\theta}{2\pi} + \frac{1}{2} \right) + \frac{\pi}{2} \tan \frac{\theta}{2} \quad (38)$$

according to Eq. (19) for the Coulomb interaction.

In the case of the linear dependence of the chemical potential on the Fermi momentum, Eq. (36) gives the well-known result for the plasmon dispersion law in gapless graphene [10]

$$\omega_{pl}(k_y) = \sqrt{\frac{g}{2} |\tilde{\mu}| \tilde{e}^2 |k_y|}. \quad (39)$$

Here, the plasmon propagates along the y axis.

The dispersion law for the two-dimensional plasmon in gapless graphene can also be obtained from Eq. (35) in the isotropic case, where $\mathbf{v}_\perp = \mathbf{v}_\parallel = \mathbf{v}_F$ and $\tilde{\mu}^2 - \Delta_{\text{eff}}^2 = \mathbf{v}_F^2 p_F^2$. Here, in the quasi-two-dimensional case, we should take into account the relation

$$p_F^2 = \frac{4\pi}{g} n_{2D}. \quad (40)$$

Formulas (34) and (35) give the well-known expressions for the case of nonrelativistic charge carriers [11]. For example, at large distances between the strips of gapless graphene ($d_{\text{II}} \gg d_I$), the system behaves as a set of strips. The Coulomb interaction between the charge carriers in one of such strips is given by the first term on the right-hand side of Eq. (18).

In the nonrelativistic limit, when $\mathbf{v}_F p_F \ll \Delta_{\text{eff}}$ and $|\tilde{\mu}| \approx \Delta_{\text{eff}}$, Eq. (34) yields

$$\omega_{pl}^{(1D)}(k_y) = |k_y| \sqrt{\frac{2g\tilde{e}^2 p_F}{\pi m^*}} \ln \frac{4}{|k_y| d_I}. \quad (41)$$

In the nonrelativistic limit for the case of isotropy with respect to velocities, formula (35) gives

$$\omega_{pl}^{(2D)}(\mathbf{k}) = \Omega_p \sqrt{|\mathbf{k}| d}, \quad (42)$$

where

$$\Omega_p = \left(\frac{2\pi \tilde{e}^2 n_{2D}}{d m^*} \right)^{1/2}. \quad (43)$$

3.4. Band Character of Plasmon Excitations

Owing to the periodicity of the array under study, not only the spectrum of single-particle excitations but also the plasmon excitation spectrum is separated into minibands. In the momentum space, the boundaries of plasmon bands coincide with the boundaries of the corresponding minibands for the charge carriers. This is a consequence of the Bragg condition: $2\mathbf{k}\mathbf{g}_j = \mathbf{g}_j^2$, $j = \pm 1, \pm 2, \dots$, where $\mathbf{g}_j = (2\pi j/d, 0)$ is the reciprocal lattice vector related to the potential of the superlattice. Thus, we find $k_{xj} = \pi j/d$.

A discontinuity appears at the boundaries of plasmon bands. Similar to [3], we can find boundary values for the plasmon frequencies.

The values of plasmon frequencies in the center of the plasmon band $\omega_{pl}(0)$ in higher minibands coincide with the minimum energy values for charge carriers in these minibands. Let us estimate these values. Finding an approximate solution of dispersion relation (3) with respect to energy at the point $k_x = k_y = 0$, we obtain

the following estimate for the energy of charge carriers in the n th miniband ($n = 0, 1, 2, \dots$):

$$E_n^{e,h} = \frac{v_F}{d_I} \left[\pm \left(\frac{\pi}{2} + \pi n \right) \left(1 - \frac{v_F}{d_I \Delta_0} \right) + \frac{V_0}{\Delta_0} \right], \quad (44)$$

where the upper and lower signs correspond to electrons and holes, respectively. In particular, estimate (44) for $n = 0$ (the lowest electron or highest hole bands) gives $E_0^{e,h} = \pm \Delta_{\text{eff}} + V_{\text{eff}}$, where Δ_{eff} and V_{eff} are specified by Eqs. (7). Let us take the characteristic values $d_I \simeq 10$ nm, $\Delta_0 \simeq 1$ eV, and $V_0 = 0$ for simplicity of estimates. Then, we have $E_0^e \simeq 80$ meV and $E_1^e \simeq 240$ meV. We can see that the energy difference between the neighboring minibands far exceeds room temperature. Hence, we can neglect the thermally activated filling of higher minibands.

Let us now estimate how many additional electrons are needed to completely fill the lowest electron miniband and to start the filling of the next electron miniband. The Fermi momentum p_F should be such that the chemical potential $\tilde{\mu}$ becomes equal to E_1^e . Using Eq. (12), we obtain $v_F p_F = \sqrt{E_1^{e2} - E_0^{e2}}$ (owing to the condition $V_0 = 0$, coincides with Δ_{eff}). Then, according to Eq. (13), we can relate the found p_F value to the two-dimensional electron density, $n_{2D} = g \sqrt{E_1^{e2} - E_0^{e2}} / (\pi v_F d) \simeq 5 \times 10^{12}$ cm $^{-2}$. This value is fairly large as compared to the experimental data for gapless graphene [10].

3.5. Absorption Intensity for the Modulated Electromagnetic Radiation

The intensity of absorption for electromagnetic waves modulated with the period equal to the plasmon wavelength is given by the well-known formula

$$Q = \frac{1}{2} \text{Re} \left(\sigma \tilde{\mathcal{E}} \mathcal{E}^* \right), \quad (45)$$

where σ is the conductivity of the system, $\tilde{\mathcal{E}}$ is the electric field of the plasmon wave, and \mathcal{E} is the electric field of the electromagnetic wave varying with the frequency ω .

The conductivity of the system is easily found from the kinetic equation in the τ approximation. In the quasi-one-dimensional case, it reads

$$\sigma^{(1D)} = \frac{ig e^2 v_F p_F}{\pi |\tilde{\mu}| (\omega + i\nu)}. \quad (46)$$

Here and further on, $\nu = 1/\tau$.

In the quasi-two-dimensional case, the conductivity is a tensor with diagonal elements

$$\begin{aligned} \sigma_{xx}^{(2D)} &= \frac{ig e^2}{4\pi(\omega + i\nu)} \frac{\tilde{\mu}^2 - \Delta_{\text{eff}}^2}{|\tilde{\mu}|} \frac{v_{\perp}}{v_{\parallel}}, \\ \sigma_{yy}^{(2D)} &= \frac{ig e^2}{4\pi(\omega + i\nu)} \frac{\tilde{\mu}^2 - \Delta_{\text{eff}}^2}{|\tilde{\mu}|} \frac{v_{\parallel}}{v_{\perp}}. \end{aligned} \quad (47)$$

In the quasi-one-dimensional case, the absorption intensity is

$$Q^{(1D)} \simeq \sigma_0^{(1D)} \mathcal{E}_0^2 \frac{\omega^2 \nu^2}{(\omega^2 - \omega_0^2)^2 + \omega^2 \nu^2}, \quad (48)$$

where $\sigma_0^{(1D)}$ is the value of conductivity (46) in the zero-frequency limit, $\omega_0 = \omega_{pl}^{(1D)}(k_0)$ is the plasmon frequency corresponding to the wave vector $\mathbf{k}_0 = (0, k_0)$, and \mathcal{E}_0 is the electric field amplitude.

In the quasi-two-dimensional case, the anisotropy of the conductivity leads to the dependence of absorption on the orientation of the polarization plane in the incident electromagnetic wave. Let its polarization plane be rotated by the angle φ with respect to the x axis. Then, the absorption intensity is equal to

$$Q^{(2D)} = Q_{\perp}^{(2D)} \cos^2 \varphi + Q_{\parallel}^{(2D)} \sin^2 \varphi. \quad (49)$$

Here,

$$\begin{aligned} Q_{\perp}^{(2D)} &\simeq \frac{1}{2} \sigma_{xx0}^{(2D)} \mathcal{E}_0^2 \frac{\omega^2 \nu^2}{(\omega^2 - \omega_0^2)^2 + \omega^2 \nu^2}, \\ Q_{\parallel}^{(2D)} &\simeq \frac{1}{2} \sigma_{yy0}^{(2D)} \mathcal{E}_0^2 \frac{\omega^2 \nu^2}{(\omega^2 - \omega_0^2)^2 + \omega^2 \nu^2}, \end{aligned} \quad (50)$$

where $\sigma_{xx0}^{(2D)}$ and $\sigma_{yy0}^{(2D)}$ are the expressions for the diagonal elements of conductivity tensor (47) in the zero-frequency limit and $\omega_0 = \omega_{pl}^{(2D)}(\mathbf{k}_0)$ is the plasmon frequency corresponding to wave vector $\mathbf{k}_0 = (k_0 \cos \varphi, k_0 \sin \varphi)$.

It follows from Eqs. (50) that the spectrum of absorption of electromagnetic waves by plasmons should be strongly anisotropic: the corresponding ratio of intensities is $Q_{\perp}^{(2D)}/Q_{\parallel}^{(2D)} = (v_{\perp}/v_{\parallel})^2$. Such strong anisotropy could be easily revealed in an experiment.

4. CONCLUSIONS

In this work, we have explicitly derived the plasmon dispersion law for the planar graphene superlattice. It has been shown that the absorption spectrum for linearly polarized electromagnetic waves modulated with the period equal to the plasmon wavelength should exhibit a pronounced anisotropy. When the Fermi level falls within the minigap, this anisotropy is due to the exclusion of oscillations of the charge carrier density across the superlattice potential. When the Fermi level falls into the miniband, this anisotropy is attributed to an appreciable suppression ($\sim (v_{\perp}/v_{\parallel})^2$) of such oscillations because of a significant difference between the transverse and longitudinal velocity components.

We are grateful to D. N. Sob'yanin for helpful discussions and valuable comments.

References

- [1] M. Freitag, T. Low, W. Zhu, H. Yan, F. Xia, and P. Avouris, *Nature Commun.* **4**, 1951 (2013).
- [2] S. Das Sarma and E.H. Hwang, *Phys. Rev. Lett.* **102**, 206412 (2009).
- [3] A.V. Chaplik, *JETP Lett.* **100**, 262 (2014).
- [4] D.C. Elias, R.R. Nair, T.M.G. Mohiuddin, S.V. Morozov, P. Blake, M.P. Halsall, A.C. Ferrari, D.W. Boukhvalov, M.I. Katsnelson, A.K. Geim, and K.S. Novoselov, *Science* **323**, 610 (2009).
- [5] I. Zanella, S. Guerini, S.B. Fagan, J.M. Filho, and G.S. Filho, *Phys. Rev. B* **77**, 073404 (2008).
- [6] S.Yu. Glazov, A.A. Kovalev, and N.E. Meshcheryakova, *Semiconductors* **49**, 504 (2015).
- [7] S.Yu. Glazov, A.A. Kovalev, and N.E. Meshcheryakova, *Bull. Russ. Acad. Sci.: Phys.* **76**, 1323 (2012).
- [8] P.V. Ratnikov, *JETP Lett.* **90**, 469 (2009).
- [9] P.V. Ratnikov and A.P. Silin, *JETP Lett.* **100**, 311 (2014).
- [10] V.N. Kotov, B. Uchoa, and V.M. Pereira, F. Guinea, and A.H. Castro Neto, *Rev. Mod. Phys.* **84**, 1067 (2012).
- [11] E.A. Andryushin and A.P. Silin, *Phys. Solid State* **35**, 164 (1993).
- [12] W. Zawadzki, *Adv. Phys.* **23**, 435 (1974).
- [13] B.L. Gel'mont and M.V. Kisin, *Sov. Phys. Semicond.* **17**, 791 (1983), *Sov. Phys. Semicond.* **17**, 947 (1983), *Sov. Phys. Semicond.* **18**, 506 (1984).
- [14] N.V. Markova, A.P. Silin, *J. Moscow Phys. Soc.* **4**, 311 (1994).
- [15] V.N. Tsytovich, *Sov. Phys. JETP* **13**, 1249 (1961).

Translated by K. Kugel